Ocean Engineering 269 (2023) 113484

Contents lists available at ScienceDirect

Ocean Engineering

journal homepage: www.elsevier.com/locate/oceaneng

Sloshing dynamics of a tuned liquid multi-column damper for semi-submersible floating offshore wind turbines

Yang Zhou, Ling Qian *, Wei Bai

Department of Computing and Mathematics, Manchester Metropolitan University, Manchester, M1 5GD, United Kingdom

ARTICLE INFO

Keywords:
Tuned liquid multi-column damper
Computational fluid dynamics
Passive control
Sloshing dynamics
Floating offshore wind turbines
OpenFOAM

ABSTRACT

In this paper, sloshing inside a novel passive control device termed tuned liquid multi-column damper (TLMCD) for mitigating rotational motions of a semi-submersible floating offshore wind turbine (FOWT) is numerically modelled using a high-fidelity CFD approach. Test cases of the device under various external excitations including single degree surge and pitch as well as combined surge/pitch are presented and analysed to reveal its damping mechanisms and performance. Through analysing the results of the predicted sloshing induced moments on the TLMCD structure and their phases under a range of external excitation frequencies, it was found that although the maximum moments always occur at or very close to the resonance excitations, their phases may not be exactly opposite to those of the wave-induced moments on a FOWT platform, which has important implications to the optimal design of the TLMCD system for floating wind turbine applications. The study also shows that the performance of the TLMCD is not significantly affected by the change of the relative angular (yaw) position of the device under pitch excitations and would potentially be more robust than the traditional U-shaped TLCDs, applied in isolation or in combination.

1. Introduction

The offshore wind industry has experienced significant growth recently and continues to expand both in the UK and worldwide. According to a recent report on offshore wind development in Europe (Ramírez et al., 2020), 25 GW of offshore wind capacity has been installed across 11 countries in the continent. Based on a pre-COVID-19 forecast (WindEurope, 2019), by 2050, 450 GW of offshore wind will be installed, accounting for almost 30% of Europe's annual electricity demand. However, nearly all of the offshore wind turbines installed to date are located in relatively shallow water and mounted on fixed bottom support structures. Given the limited availability of suitable shallow water sites with high wind resources and to reduce the environmental and visual impact of wind turbines, it is necessary to develop floating offshore wind turbine (FOWT) systems in deeper water as demonstrated in the Hywind project in Scotland, UK.

Of the three basic concepts for FOWTs (semi-submersible, tension leg platform (TLP) and spar), semi-submersible has recently received significant attention for its relatively shallow draft that improves site flexibility and installation cost-effectiveness (Trust, 2015; Robertson et al., 2014; Allen et al., 2020). However, FOWTs using semi-submersible support substructure may suffer from unacceptably large translational and rotational motions due to the resonant response of their structures and the action of extreme waves (Butterfield et al., 2007). Those external excitations may increase the system downtime, adversely affect the turbine performance and cause damage to the system components, including moorings and anchors. To prevent the potential large vertical motion, anti-heave plates, with their favourable hydrodynamic properties providing significantly enhanced system mass (added mass) and viscous damping without increasing support structure size, have been widely applied and proven effective for FOWTs with semi-submersible substructures (Lopez-Pavon and Souto-Iglesias, 2015). Therefore, it is important to explore means of mitigating wave induced and potentially large rotational motions of semi-submersible FOWTs with cost-effective control techniques to improve their performance with extended lifespan.

On the other hand, owing to the relatively low installation and maintenance costs, passive motion control devices such as tuned mass dampers (TMDs) and tuned liquid dampers (TLDs) or tuned liquid column dampers (TLCDs) have found wide use in traditional civil engineering structures (Sakai, 1989), marine vessels (anti-roll tanks for stabilising a ship's roll motion) (Holden and Fossen, 2012) and recent

* Corresponding author.
E-mail address: L.Qian@mmu.ac.uk (L. Qian).

https://doi.org/10.1016/j.oceaneng.2022.113484
Received 15 October 2022; Received in revised form 5 December 2022; Accepted 19 December 2022
Available online 3 January 2023

applications in wind turbines to suppress tower and blade vibrations through either blade or tower mounted dampers (Murtagh et al., 2008). A TLCD, which is usually a U-shaped water tank, works through the motion of its liquid column to counteract the external forces (moments) acting on a structure, and for the device to be effective, the natural frequency of a TLCD needs to be tuned to the natural frequency of the structure. The applications of TLDs and their modelling and optimisation have been discussed by many researchers through analytical, numerical and experimental approaches (Sun et al., 1992; Yu et al., 1999; Ruiz et al., 2016; Cammelli et al., 2016). In (Sun et al., 1992), Sun et al. developed a nonlinear model based on the shallow water theory for predicting the performance of a rectangular TLD under breaking wave conditions. In Yu et al. (1999), a new approach to modelling a TLD was proposed, in which equivalent tuned mass damper with non-linear stiffness and damping was used to predict the effects of the TLD under large amplitude excitations. In (Ruiz et al., 2016), Ruiz et al. developed a new type of TLD, in which a floating roof was incorporated into a traditional TLD to suppress wave breaking and higher sloshing vibration modes, and its performance was examined by scaled model tests and linear-theory based numerical models. Similarly, the effectiveness of applying TLCDs to mitigate wind-induced vibration of a high-rise building was investigated in (Cammelli et al., 2016) through both physical model tests and computational fluid dynamics (CFD) modelling.

More recently, attempts have been made to adapt TLCDs and apply them to suppress wave-induced rotational motions of FOWTs with semi-submersible support platforms. Coudurier et al. (2018) proposed a novel passive damping device called tuned liquid multi-column damper (TLMCD) by extending the number of inter-connecting vertical columns to 3 or more and incorporated it into a hypothetical semi-submersible FOWT with a barge type floater. A coupled analysis of the floater-damper system has been performed based on the developed dynamic models, which demonstrated that the TLMCD performed better than multiple TLCDs on a floater in terms of its robustness against the incident waves. To further study the flow dynamics of the TLMCD, Yu and Cheng (Yu and Cheng 2020) applied a computational fluid dynamics model to simulate the free decay of the liquid columns inside the device and the results are used to determine the natural frequencies and damping coefficients of the system and to validate an analytical model for modelling its sloshing dynamics. In (Zhou et al., 2022a), Zhou et al. validated a CFD model based on OpenFOAM and applied it to model internal sloshing inside a TLMCD system under the prescribed pitch motion and its coupling with a semi-submersible FOWT in waves. The preliminary results showed that the TLMCD as a passive control device can significantly reduce the pitch motion of the FOWT when tuned to the pitch resonant frequency of the floater. Xue et al. (2022) applied a similar numerical model to evaluate the effects of an integrated TLMCD on the pitch motion of a semi-submersible FOWT in regular wave conditions and compared it with the experimental measurements. The study further demonstrated that an optimised damping effect can be achieved near the pitch resonance frequency, where the maximum pitch motion could be reduced by around 18%.

Although limited experimental and numerical investigations have been conducted to demonstrate the effectiveness of a TLMCD in reducing the pitch motion of a semi-submersible FOWT platform, no detailed analysis of the sloshing dynamics of the new TLMCD device under realistic external excitations can be found in the literature. Such work will be important for revealing the damping mechanisms of the device for semi-submersible FOWTs and ultimately providing guidance on their optimal design. To achieve this goal, in this study, the CFD model developed by the authors (Zhou et al., 2022a) is further validated for internal sloshing problems of TLCDs against other numerical and experimental results in terms of the sloshing-induced moments and their phase differences over a range of excitation frequencies. It is then applied to model sloshing inside a TLMCD designed for a specific FOWT support structure under various external excitations including single degree pitch and surge motions as well as combined pitch and surge motions. Particular attention has been paid to the analysis of the sloshing dynamics of the new passive damping system, including the effects of excitation frequencies and amplitudes on the sloshing induced moments (both amplitude and phase) on the structure. Finally, to examine the potential effects of wave incidence in its performance, sloshing inside the passive damping device with changed yaw positions under the pitch motion is also simulated, along with a summary of the main findings from the current work.

2. Numerical method

2.1. The flow model

2.1.1. Governing equations

To model the flow problem of liquid sloshing inside a TLMCD, the multiphase flow solver in the open-source CFD framework OpenFOAM (OpenFOAM, 2019) has been adopted in this work. The flow inside the TLMCD system consisting of water and air, as well as their interfaces, is assumed to be incompressible, transient and viscous, and is governed by the continuity and unsteady Reynolds-averaged Navier-Stokes (RANS) equations,

$$\nabla \bullet \boldsymbol{U} = 0 \tag{1}$$

$$\frac{\partial \rho \boldsymbol{U}}{\partial t} + \nabla \bullet \left(\rho\left(\boldsymbol{U} - \boldsymbol{U}_g\right)\boldsymbol{U}\right) = -\nabla P_t - \boldsymbol{g} \bullet \boldsymbol{x} \nabla \rho + \nabla\left(\mu_{eff} \nabla \boldsymbol{U}\right) + (\nabla \boldsymbol{U}) \bullet \mu_{eff} + \boldsymbol{f}_\sigma \tag{2}$$

where $\nabla = \left(\frac{\partial}{\partial x}, \frac{\partial}{\partial y}, \frac{\partial}{\partial z}\right)$ is the gradient operator, $\boldsymbol{U}$ and $\boldsymbol{U}_g$ are the velocities of the fluid flow and the grid nodes in Cartesian coordinates, respectively, ρ is the density of water and air mixture, $\boldsymbol{g}$ denotes the gravity acceleration vector and $P_t = P - \rho \boldsymbol{g} \bullet \boldsymbol{x}$ is the hydrodynamic pressure obtained by the total pressure P minus the hydrostatic pressure $\rho \boldsymbol{g} \bullet \boldsymbol{x}$. The formula $\mu_{eff} = \rho\ (\nu + \nu_t)$ is used to calculate the effective dynamic viscosity, in which ν and ν_t are the kinematic and eddy viscosity, respectively; the surface tension term $\boldsymbol{f}_\sigma$ is included here for completeness of the equations and its effects can be ignored in the current simulations.

2.1.2. Free surface modelling

To model the free surface flow problem involving water and air, the widely adopted Volume of Fluid (VOF) (Hirt and Nichols, 1981) method is used to identify the two phases and their interface by introducing the volume fraction function α. The value of α is between 0 and 1 and for air $\alpha = 0$ and for water $\alpha = 1$. The evolution of the volume fraction can be described by the following equation:

$$\frac{\partial \alpha}{\partial t} + \nabla \bullet \left[\left(\boldsymbol{U} - \boldsymbol{U}_g\right)\alpha\right] + \nabla \bullet \left[\boldsymbol{U}_r(1-\alpha)\alpha\right] = 0 \tag{3}$$

It should be noted here that to maintain a sharp interface between water and air, an additional compression term has been added to the left-hand side of the transport equation, where $\boldsymbol{U}_r = \boldsymbol{U}_{water} - \boldsymbol{U}_{air}$ is an artificial velocity field and it only takes effect in the transitional region between water and air due to the inclusion of the factor $(1-\alpha)\alpha$.

For a multiphase flow problem, the value of the volume fraction is used as the weighting factor to calculate the mixture properties. Listed below are the equations for calculating the density and the viscosity of the water and air mixture,

$$\rho = \alpha \rho_w + (1-\alpha)\rho_a \tag{4}$$

$$\mu = \alpha \mu_w + (1-\alpha)\mu_a \tag{5}$$

where the subscripts w and a represent water and air respectively.

Table 1
Geometries and initial water levels of the U-shaped TLCD water tank.

H (m)	V_{CoR} (m)	V (m)	V_d (m)	A_H (m^2)	A_V (m^2)	L (m)
12.800	1.372	1.524	0.160	3.254	14.631	5.334

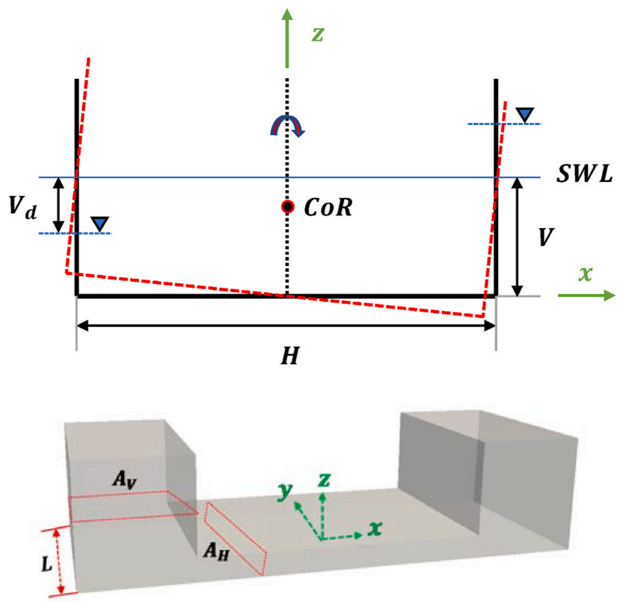

Fig. 1. Sketch of the U-shaped TLCD, top: 2D plot in XoZ plane, bottom: 3D TLCD configuration.

2.2. Numerical implementation

The OpenFOAM multiphase solver "interFoam" is utilised to perform all the simulations, in which the pressure velocity coupling is achieved through the PIMPLE algorithm (a combination of PISO: Pressure Implicit with Splitting of Operators and SIMPLE: Semi-Implicit Method for pressure-linked Equations). Further details on the numerical implementation in OpenFOAM can be found in (OpenFOAM, 2019; Zhou et al., 2021; Zhou et al., 2022b). To run a typical case of liquid sloshing in a three-column TLMCD for 1300 s (around 50 excitation periods), it takes about 17 h on a CPU cluster of 180 cores running in parallel. Details of the computational domain and boundary conditions are provided in the following sections.

3. Validation and verification

To check the accuracy of the numerical model for internal liquid sloshing problems, three sets of test cases involving a simplified U-shaped TLCD and three-column star-like TLMCD are modelled, which include an internal liquid (water) free-decay test to calibrate the natural angular frequency of the system, the liquid sloshing inside a TLCD under prescribed roll motion and an internal liquid free-decay test for three-column star-like TLMCD.

3.1. Transient decay of U-shaped TLCD

The U-shaped TLCD has the dimensions which are shown in Table 1 and Fig. 1. For the natural angular frequency calibration, the initial water levels in the right and left columns are set at a height of V_d above and below the SWL (Still Water Level) respectively. Under the effects of gravity and fluid viscosity, the water columns will undergo oscillatory motion while their levels will finally approach the value of SWL, i.e., V =1.524 m. To determine an appropriate mesh size for the flow problem, a mesh convergence test was carried out using three levels of meshes, i.e., fine (100.4 k cells); medium (76.3 k cells); coarse (61.8 k cells). For the simulations, no-slip boundary condition is applied at the internal walls of U-shaped TLCD and the atmospherical condition is applied at the two top openings of the vertical columns. The results in Fig. 2 show that with sufficiently refined meshes, the predicted natural angular frequency of the oscillating water column as well as its decay rate are not sensitive to mesh sizes. The value of the predicted natural angular frequency is 0.669 rad/s that is close to the analytical result of 0.648 rad/s based on potential flow theories.

3.2. The prescribed roll motion of U-shaped TLCD

Next, water sloshing in the U-shaped TLCD under prescribed harmonic rotational (roll) motions around the centre of rotation (y-axis, CoR), as shown by the red dashed line in the top diagram of Fig. 1, is simulated. The amplitude of the roll motion is set at 2° and the excitation frequency varies from 0.3 rad/s to 1.0 rad/s, which is set around the natural angular frequency (0.669 rad/s) of the TLCD system. For the simulations, the same initial numerical setup including the mesh has been applied. The maximum allowed Courant number is 0.7, and the initial time step is 1/2000T, which T refers to the period of the roll motion. From the simulation results, the amplitude of the roll moment around the y-axis is calculated and compared with the experimental measurements and the results from other numerical approaches (Kerkvliet et al., 2014; Thanyamanta and Molyneux, 2012) as shown in Fig. 3. Generally, the current results agree well with other CFD results although all the CFD results slightly under-predict the roll moment amplitudes for all frequencies and over-predict the phase lag between the frequency range of 0.65 and 0.8 rad/s. Additionally, it can be observed from Fig. 3 that the maximum roll moment is reached at or very close to the natural angular frequency (0.669 rad/s) of the TLCD system and with the increase in the oscillation frequency, the phase lag, which is defined as the difference between the phase of the roll moment due to water sloshing and that of the external excitation, can be calculated from the difference between the zero-upcrossing time instant and the start of each prescribed motion cycle, will increase from 0 deg to 180

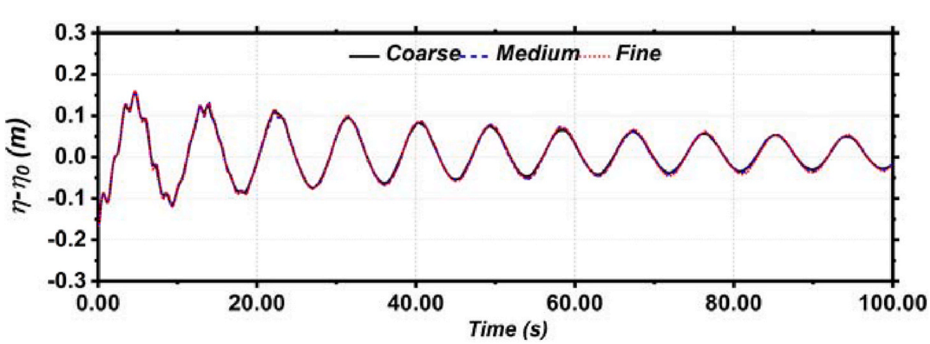

Fig. 2. Water surface level at the left column of the U-shape TLCD, η_0 (1.524m) refers to the initial water level.

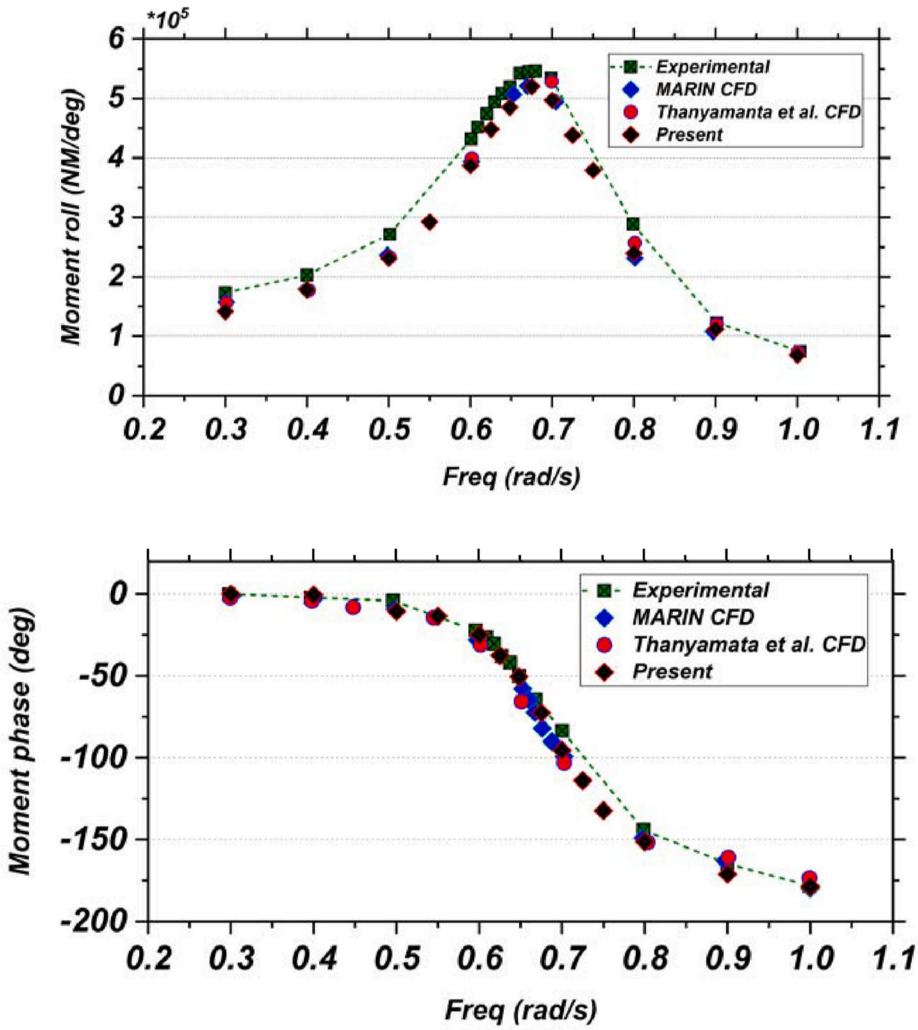

Fig. 3. Comparisons of the roll moment amplitude and phase for U-shaped TLCD.

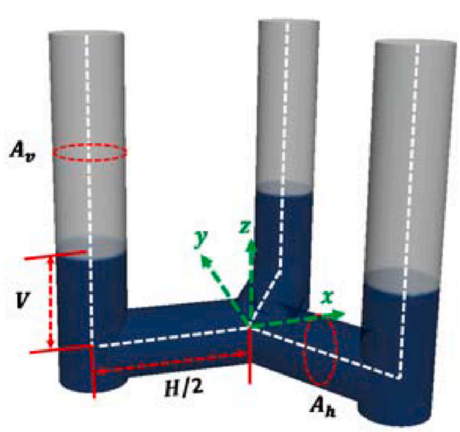

Fig. 4. Sketch of the three-column star-like TLMCD.

Table 2
Geometries of the star-like TLMCD.

H (m)	V_{CoR} (m)	V (m)	A_h (m^2)	A_v (m^2)	Rm (%)
56.10	4.50	6.00	8.04	50.24	5.86

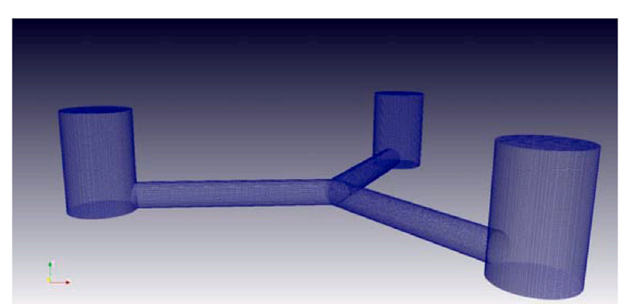

Fig. 5. Computational mesh for the TLMCD under the medium mesh arrangement.

deg. As discussed in the results section, the phase lag plays a key role in determining the effectiveness of TLCDs in mitigating roll motions of floating structures.

3.3. *Transient decay of three-column star-like TLMCD*

In this section, free decay of water columns inside a three-column star-like TLMCD (Yu and Cheng 2020) is simulated and the key parameters are provided in Fig. 4 and Table 2, where V_{CoR} refers to the vertical height from the bottom of the TLMCD to the CoR, Rm represents the ratio of the liquid mass inside the TLMCD to the mass of the OC4

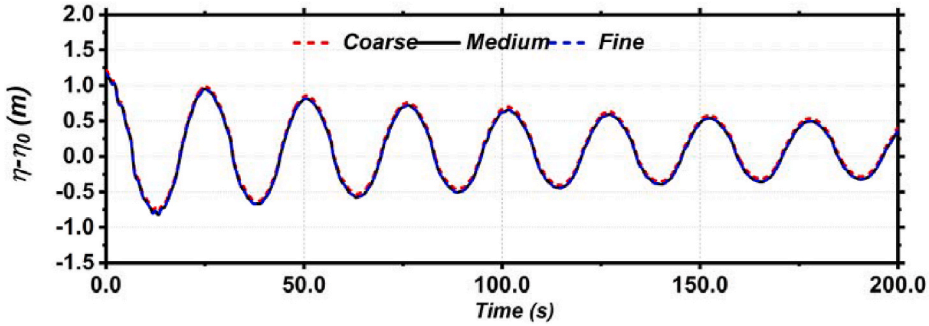

Fig. 6. Free surface level at the left column of the TLMCD, η_0 (6.0m) refers to its water level at the equilibrium state.

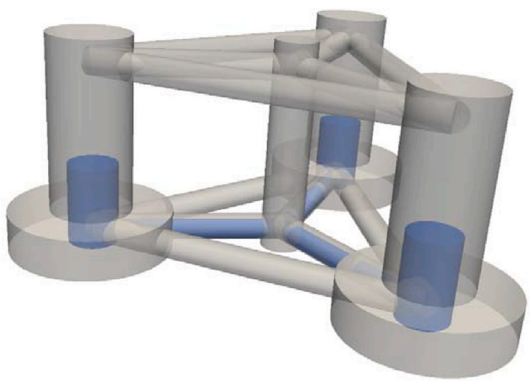

Fig. 7. Sketch of the three-column star-like TLMCD and semi-submersible platform.

semi-submersible platform (Robertson et al., 2014). The natural frequency of the TLMCD system was compared with the analytical data via a transient decay test, where the initial water levels in different columns were 7.26 m, 5.37 m, and 5.37 m, respectively.

A mesh convergence test is carried out to determine the appropriate mesh sizes for the flow problem. Three meshes with different densities are used in the current study: fine (103k cells); medium (81k cells); coarse (49k cells). The mesh is generated using the built-in mesh generation tool "snappyhexmesh" in OpenFOAM and Fig. 5 shows the generated unstructured mesh for the TLMCD under the medium mesh arrangement. Five layers of boundary layer mesh with the first layer grid thickness of 0.5 mm and a stretching factor of 1.2 are introduced. This is to ensure that the flow separation near the sharp corners is well captured in the simulation. The applied boundary conditions for the flow problem are the same as those for the U-shaped TLCD. The mesh convergence studies in Fig. 6 show that with a sufficiently fine mesh, the angular frequency for the transient decay is not sensitive to different mesh sizes and agree well with the analytical results: $\omega = 0.233$ rad/s or $T = 26.96$ s, calculated from the following formula:

$$\omega = \sqrt{\frac{2 * g}{\mathrm{H} * \frac{A_V}{A_H} + 2 * \mathrm{V}}} \tag{6}$$

4. Case studies

4.1. Design of TLMCDs for semi-submersible FOWT platforms

To illustrate how a TLMCD system can be incorporated into a FOWT support structure, the NREL OC4 semi-submersible platform (Robertson et al., 2014) is used as an example. As shown in Fig. 7, a star-like TLMCD is designed based on the configuration of its substructure, i.e., the sizes of its offset columns and the crossing braces, and the total mass of the semi-submersible platform. As with other TLCD systems, the natural angular frequency of the TLMCD system i.e., $\omega = 0.233$ rad/s has been tuned (based on Eq. (6)) to be the same as or very close to that of the OC4 semi-submersible platform pitch natural frequency. Note that to achieve this objective for the TLMCD system, the radius of the crossing braces of the semi-submersible support structure has been slightly increased. The gross properties of the TLMCD are given in Table 2 - the lengths of the horizontal and vertical water columns are 56.1 m and 6 m, and the radius of the horizontal and vertical cross-sections are 1.6 m and 4.0 m, respectively.

4.2. Test cases

In this study, four sets of load cases are examined to reveal the sloshing dynamics and responses of the TLMCD as a passive control device for semi-submersible FOWTs. The configuration of the TLMCD as defined in Table 2 is used in the simulations.

As the TLMCD is designed to reduce the rotational motions of FOWTs and therefore, the prominent degree of freedom (DoF) is the pitch motion, water sloshing inside the TLMCD under the prescribed harmonic

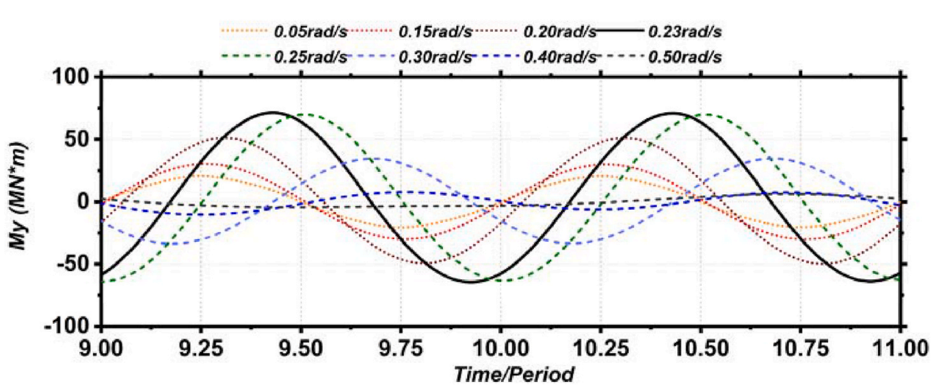

Fig. 8. Pitch moment predictions of the three-column star-like TLMCD under pitch excitation.

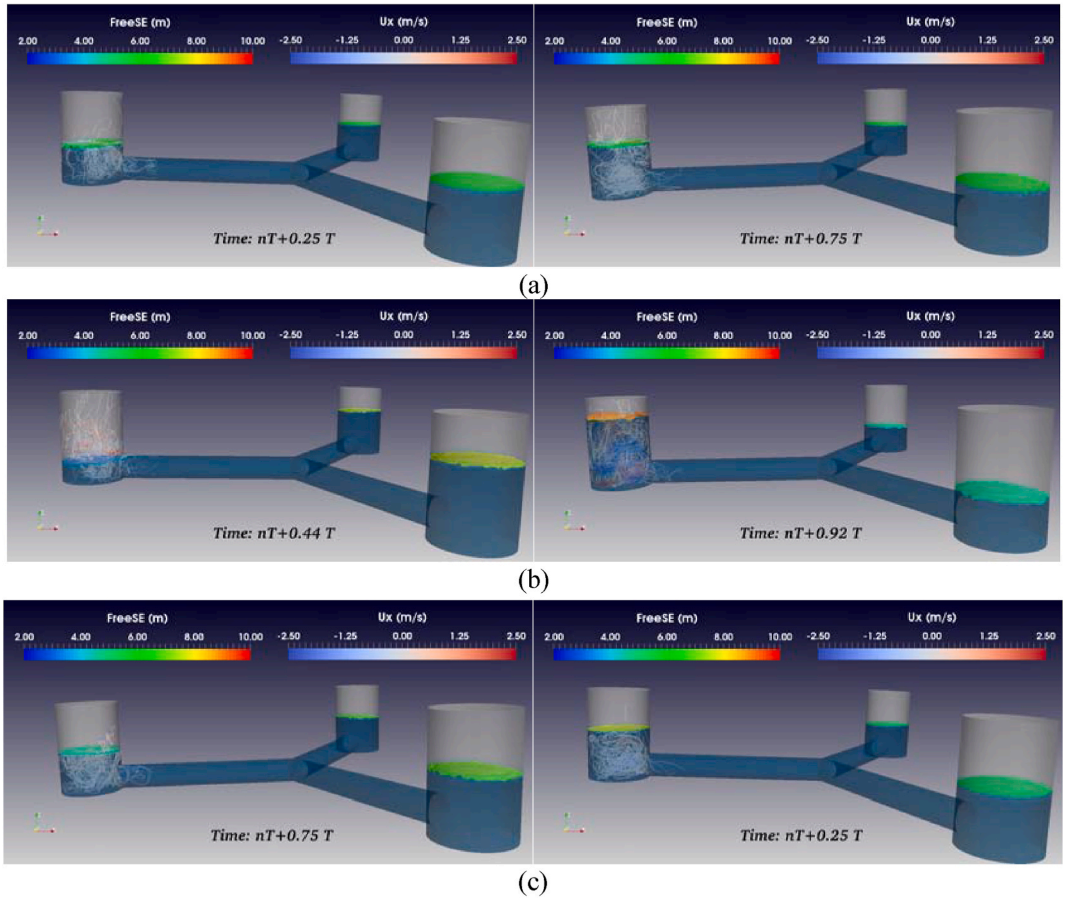

Fig. 9. Surface elevation contour plots inside the TLMCD under different excitations (a) 0.05 rad/s (b) 0.23 rad/s (c) 0.4 rad/s with prescribed pitch motion.

pitch excitation will be examined first. The angular frequency of the pitch oscillations ranges from 0.05 rad/s to 0.5 rad/s and the amplitude is set as 2° based on the motion RAO of the semi-submersible FOWT under normal sea states. Furthermore, as FOWTs will experience both translational and rotational motion in real sea states, liquid sloshing under surge only (with an amplitude of 4 m) and combined surge and pitch motions will be simulated to investigate the sloshing dynamics of the TLMCD under realistic external excitations. Additionally, to examine the robustness of the TLMCD system in response to incident wave directions the TLMCD under combined pitch and roll motions will be also studied. Finally, the impact of the excitation amplitude on the response of the TLMCD will be investigated and this is to analyse the sloshing hydrodynamics of the device under different wave conditions, including the extreme sea states.

5. Results and discussions

5.1. Sloshing under prescribed external excitations

5.1.1. Pitch motion only case

Fig. 8 shows the time history of the sloshing induced pitch moment of the three-column star-like TLMCD between the sampled oscillation periods (from 9T to 11T) for the eight selected excitation frequencies ranging from 0.05 rad/s to 0.5 rad/s. From Fig. 8, it can be observed that when the external excitation frequency is close to the natural frequency of the TLMCD system (resonant frequency), i.e., $\omega = 0.23$ rad/s, the amplitude of the pitch moment reaches a maximum value of nearly 76 MNm. In terms of the phase lag, its value increases from 0° at the low excitation frequency to 180° at the high excitation frequency. Close to the resonant frequency, the phase lag is sensitive to the frequency of external excitation, e.g., under the resonant excitation ($\omega = 0.23$ rad/s), the phase lag $\varphi = (9.17 - 9.00) \times 2\pi = 1.068$ rad $= 61.2$ degrees while it is about 90° when $\omega = 0.25$ rad/s. Generally, the sloshing dynamics of the TLMCD under a prescribed pitch only motion resembles that of the U-shaped TLCD, as presented in Fig. 3.

Consider when the TLMCD system is incorporated into a semi-submersible FOWT platform, under wave excitations at or close to the resonance frequency, the phase lag between the hydrodynamic force and dynamic motion of the FOWT is about 90°, and if the phase lag between the dynamic motion of FOWT (the prescribed motion of TLMCD in the current case) and the restoring moment induced by the internal sloshing is also around 90°, then the phase lag between the internal restoring moment and wave hydrodynamic moment will be close to 180°. In other words, the sloshing induced moment from a TLMCD will cancel out part of the wave induced moment on the structure and hence a reduced rotational motion (Sun et al., 1992; Kerkvliet et al., 2014). However, from the simulation results, it can be shown that at the resonant frequency, the phase lag between the sloshing induced moment and the external excitation is quite below 90° and to achieve optimal damping for a TLMCD, a small shift from the resonant frequency might need to be applied to the natural frequency of the device.

Because the pitch moment of TLMCD under different prescribed oscillations is highly correlated with the induced frequency, the surface elevation contours with the streamlines in one of the vertical columns and its connecting region with the horizontal column (located in the negative x direction) are plotted in Fig. 9 for three different excitation frequencies, i.e., 0.05 rad/s, 0.23 rad/s, and 0.4 rad/s. Focusing on the results under the natural frequency of around 0.23 rad/s (Fig. 9 (b)), a significant surface elevation variation can be observed between the column on the left and the two columns on the right and at t = 0.92 T, a

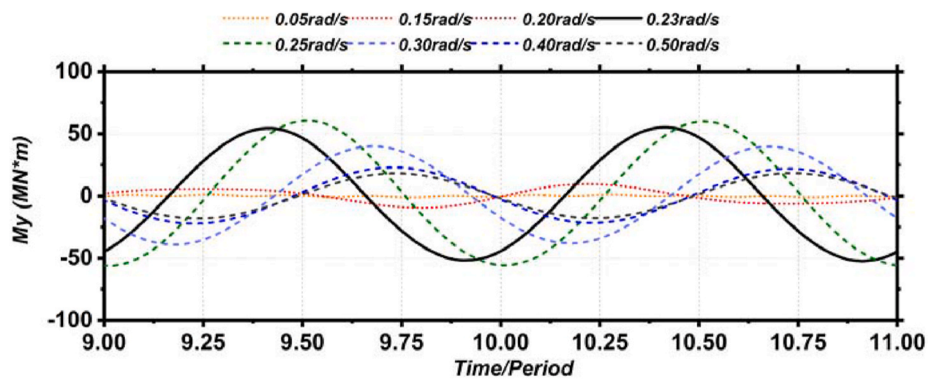

Fig. 10. Pitch moment predictions of the three-column star-like TLMCD under surge excitation.

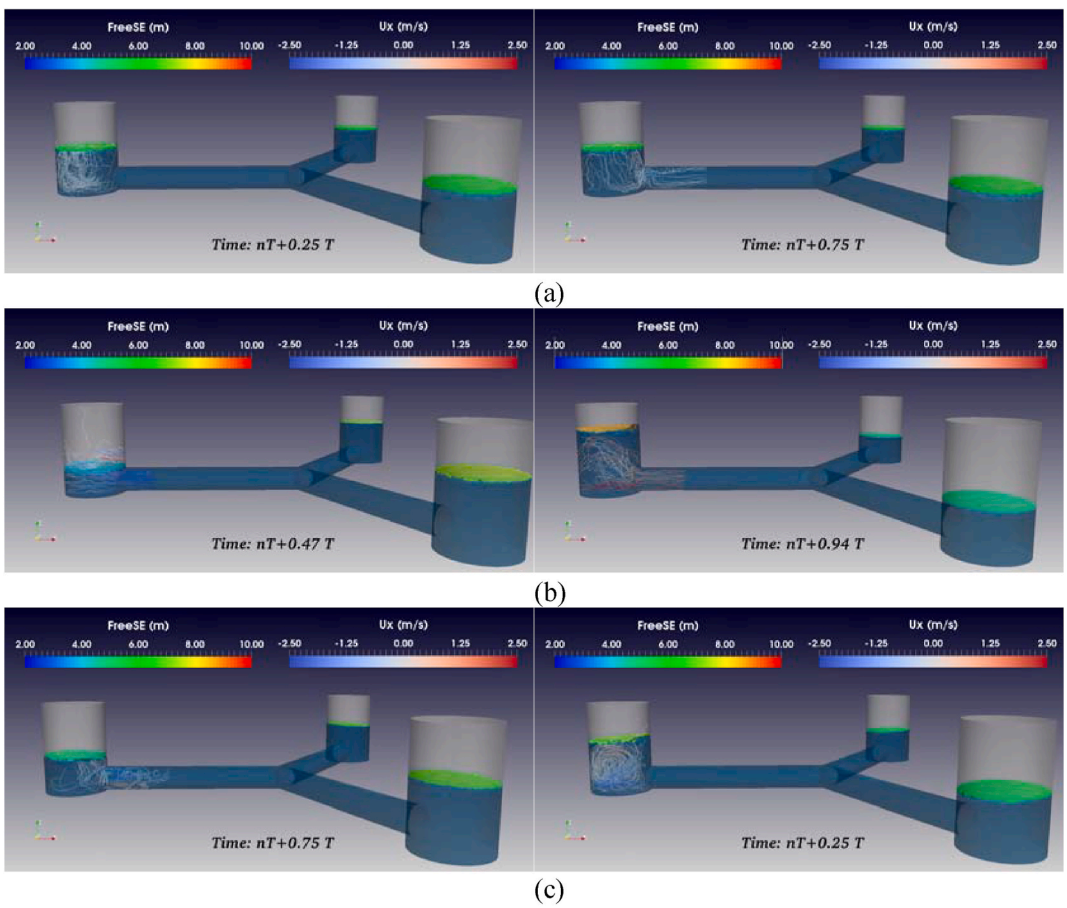

Fig. 11. Surface elevation contour plots inside the TLMCD under different excitations (a) 0.05 rad/s (b) 0.23 rad/s (c) 0.4 rad/s with prescribed surge motion.

high water level of around 9 m is reached. In contrast, the surface elevation variation is relatively small under the excitation frequencies of 0.05 rad/s and 0.4 rad/s as shown in Fig. 9 (a) and (c).

5.1.2. *Surge motion only case*

Fig. 10 plots the pitch moment under the prescribed surge motions. The pitch moment amplitude and phase lag variations under different excitation frequencies display a similar trend to the previous results under the prescribed pitch motions shown in Fig. 8. One difference that could be found is that the pitch moment is relatively smaller under low-frequency excitations than high-frequency ones, which displays an opposite trend to the results in Fig. 8 under pitch motion excitations. This is because that the difference in the surface elevation in each column induced by the surge motion is not as large as the one under the pitch motion for low frequency excitations.

The surface elevation contours under three different excitation frequencies of the prescribed surge motions are given in Fig. 11. Compared with the results shown in Fig. 9, at either low or high-frequency excitations shown in Fig. 11 (a) and (c) and Fig. 9 (a) and (c), the surface elevations in the three columns of the TLMCD under the prescribed surge motion and the prescribed pitch motion are very close to the initial surface elevation, i.e., 6 m. However, discrepancies can be observed under the natural frequency showing that the surface elevation variations between the upstream and downstream columns under the prescribed surge motion are not as significant as in the prescribed pitch motion.

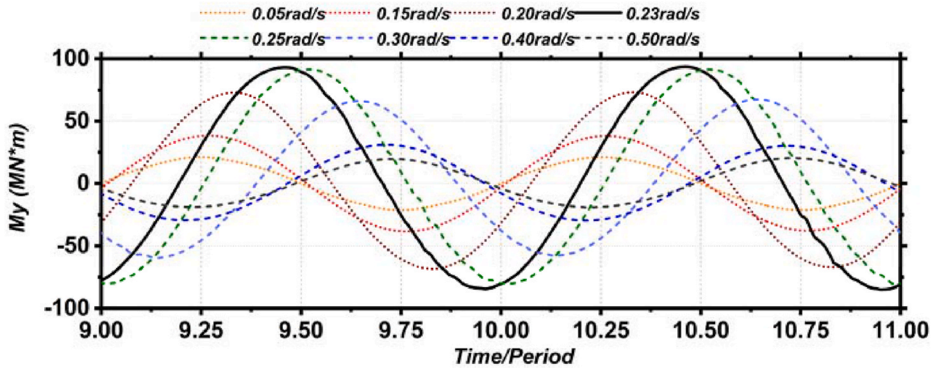

Fig. 12. Pitch moment predictions of the three-column star-like TLMCD under pitch and surge excitation.

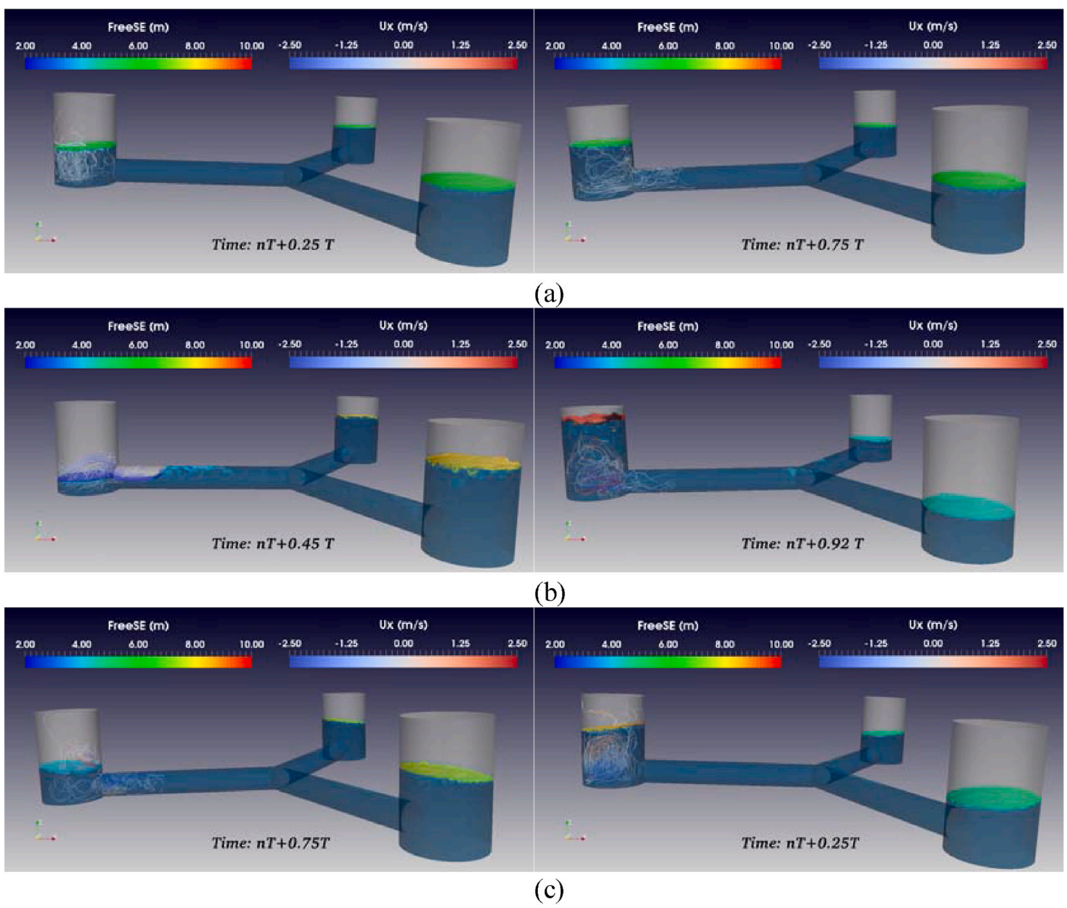

Fig. 13. Surface elevation contour plots inside the TLMCD under different excitations (a) 0.05 rad/s (b) 0.23 rad/s (c) 0.4 rad/s with the combined surge and pitch motion.

5.1.3. Surge and pitch motion case

Next, sloshing inside the TLMCD system under the prescribed translational (surge) and rotational (pitch) motion is modelled to imitate sloshing dynamics under the movement of an FOWT in waves. Focusing on the pitch moment plotted in Fig. 12, its amplitudes at the lowest or highest excitation frequencies, i.e., $f = 0.05$ rad/s and $f = 0.5$ rad/ s are close to each other at 26 MNm. Additionally, the combined surge and pitch motion result in an increase of the pitch moment amplitude to nearly 50 NMm/deg under the natural frequency excitation.

Additionally, Fig. 13 plots the surface elevation of TLMCD under three excitation frequencies, i.e., 0.05 rad/s, 0.23 rad/s, and 0.4 rad/s of the combined surge and pitch motion. Compared to the plots in Figs. 9 and 11, it is found that the combined surge and pitch motion has contributed to relatively larger water-level differences between the left and the two right columns. Specifically, from the results for the case under the natural frequency excitation (Fig. 13 (b)), the water level inside the left column can become very shallow leading to the partial filling of water in the connecting horizontal duct and this is also reflected in the nonlinear behaviour observed in Fig. 12 (black line) at 9.45T and 10.45T.

Fig. 14 (a) and (b) summarise the results of the pitch moment amplitude and phase lag for the three-column star-like TLMCD under the pitch, surge and combined pitch and surge excitations. From these results, two observations can be made. Firstly, the amplitude of the pitch moment induced by the combined surge and pitch motion is quite close to the linear superposition of the moment under the prescribed pitch

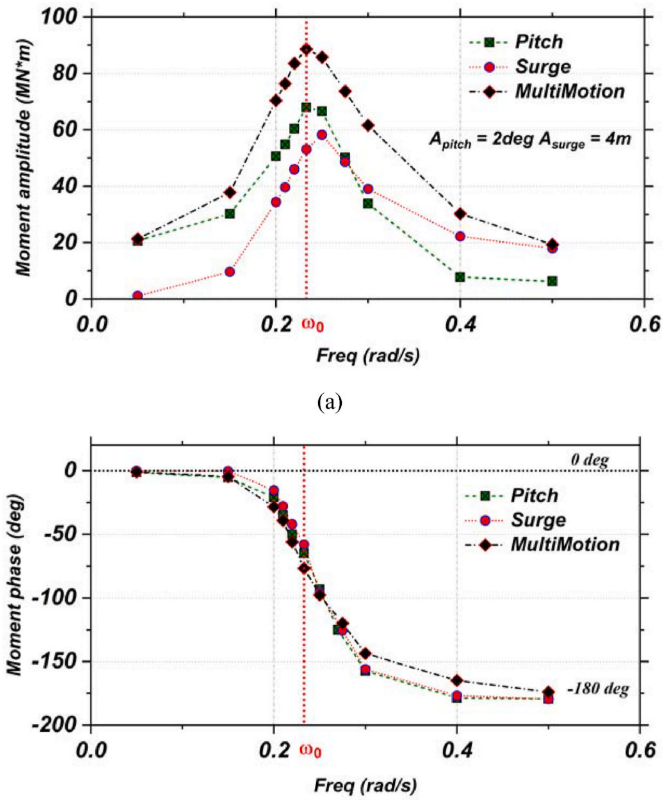

Fig. 14. Pitch moment under various external excitations; (a) Amplitude (b) Phase lag.

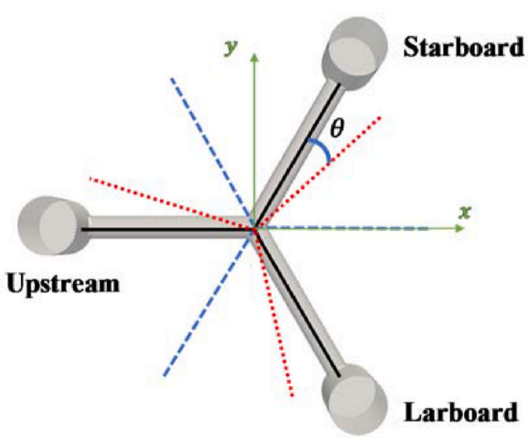

Fig. 15. Sketch of TLMCD with the different rotation angle.

only and surge only motion at either low frequency or high frequency excitation that strong nonlinearities do not occur, although the location of the maximum moment for the surge only case is slightly shifted to the right from the resonance frequency. Secondly, the phase lag in the sloshing induced pitch moment is not significantly affected by the motion types and in the region close to the resonance frequency, a phase lag of around 90° can be achieved. As discussed in the previous sections, this has critical implications for a TLMCD to be effective in reducing the wave induced rotational motions of FOWTs.

5.1.4. Effects of device yaw angles

This section is designed to assess the robustness of the three-column star-like TLMCD in providing restoring moments against the rotational motions of a semi-submersible FOWT under different incident wave directions. This is achieved through modelling sloshing inside the TLMCD with different yaw angles under the pitch excitation. As shown in Fig. 15, the angle between any two adjacent columns of the TLMCD is 120° and if the TLMCD is turned by 60° around the z-axis, the structure will be simply mirrored to the YoZ plane, resulting in identical sloshing dynamics. Therefore, to avoid duplication of test cases, the considered yaw angles of the device range from 0 deg to 30 deg. The prescribed amplitude of pitch motion is 2° and the oscillation angular frequency is set at the resonance value of 0.233 rad/s.

Focusing on the predicted pitch moments, which are plotted in Fig. 16, while they are in phase with each other, their amplitudes will slightly drop with an increase in the yaw angles. For example, only a small drop of the pitch moment amplitude from the maximum value of 69.4 MNm at the 0 degree of yaw angle can be observed for the cases of 5, 10, 15 and 20°. At 30°, the amplitude of the pitch moment reaches its lowest value of 59.6 MNm, which is around 14% smaller than the result under 0°. This can be explained by the fact that as the yaw angle is 30°, only two columns (the Upstream and Larboard columns as referred to in Fig. 15) will be most effective for providing restoring moments through water sloshing up and down.

Fig. 17 plots the surface elevation at each column of the TLMCD at five time instants, i.e., at the equilibrium position (T = 0T); the maximum pitch & roll motion (T = 0.25T); maximum pitch moment (T = 0.44T); the minimum pitch & roll motion (T = 0.75T) and the minimum pitch moment (T = 0.92T). The red dashed line represents the initial surface elevation at each column, i.e., V = 6.0 m. It can be noticed that as the yaw angle of the structure increases from 0° to 30°, the surface elevation at the starboard column moves closer to the initial water level, and more specifically, when the angle becomes 30°, sloshing will only occur between the upstream and larboard columns since the arm (connecting duct) of the starboard column is perpendicular to the incident wave direction.

The above results demonstrate that the three-column star-like TLMCD is more robust for FOWT applications as the sloshing-induced anti-rotational pitch moment is not significantly affected by the change of the yaw angle and could be a better option than U-shaped TLCDs for reducing the platform motion (Coudurier et al., 2018).

5.2. Effects of motion amplitudes

This section studies what the TLMCD will perform under different motion amplitudes to imitate its behaviour inside a semi-submersible platform under different sea states. The selected cases vary from 1 deg to 4 deg on the prescribed pitch amplitude and range from 2 m to 8 m for the prescribed surge amplitude. Fig. 18 shows the time history of the pitch moment of the three-column star-like TLMCD under one sampled period (from 10T to 11T). The instantaneous time is non-dimensionalised by the prescribed oscillation period, and the y-axis is divided by the prescribed motion amplitude. Regardless of what type of motion is prescribed on the TLMCD, we can see from Fig. 18 (a)–(c) that, under low excitation frequency (0.05 rad/s) and high excitation frequency (0.5 rad/s), the pitch moment is in a good agreement, which reveals the fact that the pitch moment increases linearly with the prescribed translational/rotational amplitude. However, it is observed that under the resonance frequency, the absolute pitch moment increases with the increase in the motion amplitude, although their per degree of rotation or per metre of translation value actually decreases. Additionally, the phase lag also increases from around 61°–82° as the prescribed motion amplitude increases. All these indicate the nonlinear behaviour of sloshing dynamics in the TLMCD under the resonant excitation.

6. Conclusion

In this paper, sloshing inside the TLMCD - a new passive control device consisting of multiple inter-connected vertical columns for

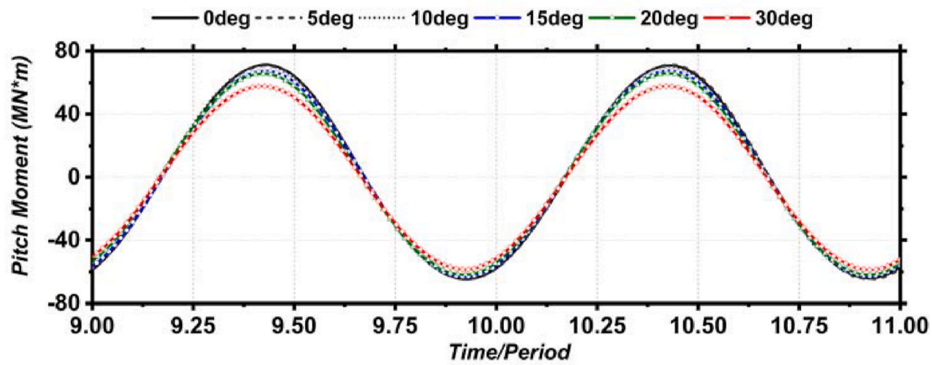

Fig. 16. Pitch moment predictions of the three-column star-like TLMCD under pitch motion with different yaw angles.

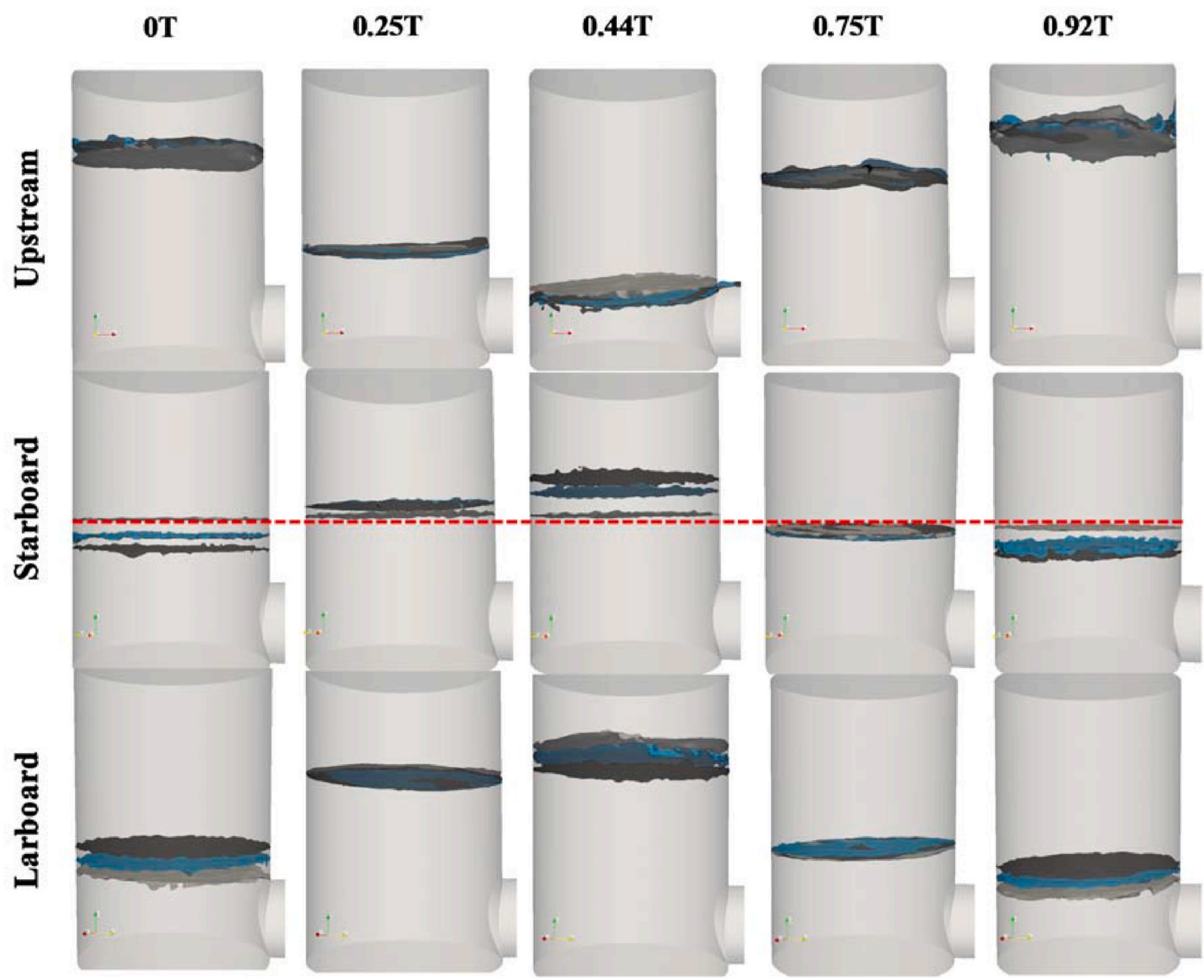

Fig. 17. Surface elevation plots of TLMCD under 0° (Black), 15° (Blue), and 30° (Grey) at different columns. (For interpretation of the references to colour in this figure legend, the reader is referred to the Web version of this article.)

mitigating the rotational motion of semi-submersible FOWTs, has been studied. This is achieved by applying a high-fidelity CFD model based on OpenFOAM to model the two-phase flow of water and air inside the damping device.

To demonstrate the applicability of the device to semi-submersible FOWTs, a specific TLMCD with three interconnected columns has been designed based on the configuration of the OC4 semi-submersible platform. Water sloshing inside the TLMCD under external hormonic excitations including surge only, pitch only, combined surge and pitch, and combined pitch and roll motions is then simulated for a range of excitation frequencies have been simulated. The results revealed that for the external excitation types, while the maximum pitch moments induced by liquid sloshing on the rotational centre of the damping device always occur at or close to the system resonant frequency, the phase lag between the maximum restoring moment and the prescribed motion is in a region much lower than 90°, which indicates that the a TLMCD that is designed based on the natural frequency of a FOWT platform might not achieve an optimal performance in terms of cancelling out the wave

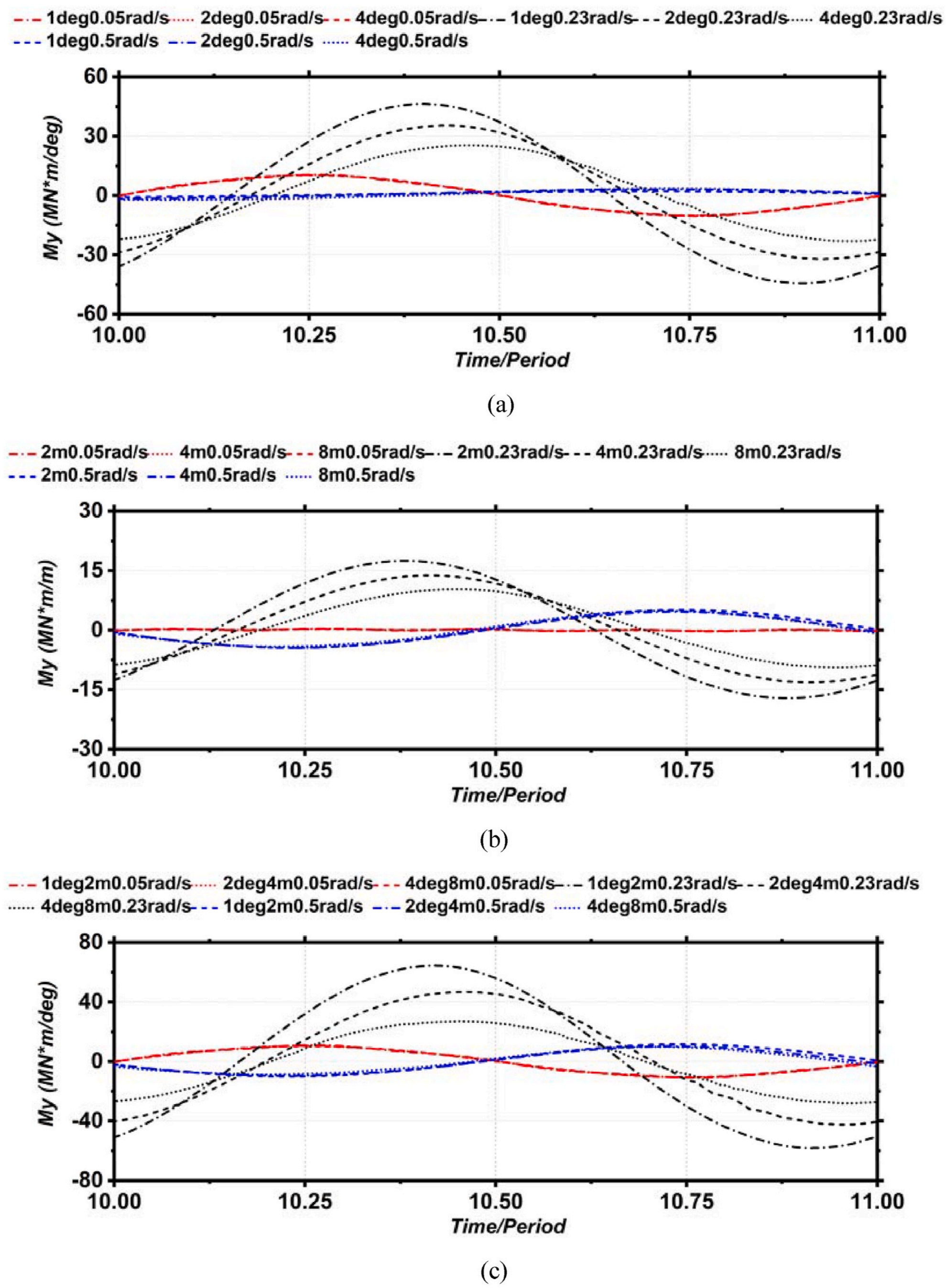

Fig. 18. Pitch moment predictions of the three-column star-like TLMCD under different motion amplitude; (a) pitch only (b) surge only (c) pitch and surge.

induced moments on its structure. Additionally, it is observed that when the excitation frequencies are away from the resonance frequency the pitch moments of the TLMCD under combined surge and pitch motions are close to the linear superposition of the individual prescribed motion. From the results of the pitch induced sloshing for different device yaw angles, it is found that the pitch moment will only decrease marginally as the yaw angle of the TLMCD increases from 0° to 30°, and the worst scenario occurs at an angle of 30°, where only the sloshing between the upstream and larboard columns will be significant and contributes to the creation of restoring moments. The results confirm that a TLMCD can be a better alternative to the use of traditional TLCDs either in isolation or in combination for floating offshore wind applications. The present work is limited to the analysis of sloshing dynamics inside the TLMCD under prescribed external excitations. To fully evaluate the effectiveness of a TLMCD in reducing FOWT platform motions, a coupled analysis of sloshing dynamics and platform motions under realistic wave and wind excitations is required and this will be carried out in the future.

CRediT authorship contribution statement

Yang Zhou: Methodology, Data curation, Software, Writing – original draft. **Ling Qian:** Funding acquisition, Conceptualization, Methodology, Supervision, Writing – review & editing. **Wei Bai:** Methodology, Supervision, Writing- Reviewing.

Declaration of competing interest

The authors declare that they have no known competing financial interests or personal relationships that could have appeared to influence the work reported in this paper.

Data availability

Data will be made available on request.

Acknowledgement

This work is funded by the SUPERGEN ORE Hub (UK) Flexible Fund project titled 'Passive Control of Wave Induced Platform Motion for Semi-submersible FOWTs'. This work used the Cirrus UK National Tier-2 HPC Service at EPCC (http://www.cirrus.ac.uk) funded by the University of Edinburgh and EPSRC (EP/P020267/1).

References

Allen, C., Viscelli, A., Dagher, H., Goupee, A., Gaertner, E., Abbas, N., Hall, M., Barter, G., 2020. Definition of the UMaine VolturnUS-S Reference Platform Developed for the IEA Wind 15-megawatt Offshore Reference Wind Turbine. National Renewable Energy Lab.(NREL), Golden, CO (United States).

Butterfield, S., Musial, W., Jonkman, J., Sclavounos, P., 2007. Engineering Challenges for Floating Offshore Wind Turbines. National Renewable Energy Lab.(NREL), Golden, CO (United States).

Cammelli, S., Li, Y.F., Mijorski, S., 2016. Mitigation of wind-induced accelerations using tuned liquid column dampers: experimental and numerical studies. J. Wind Eng. Ind. Aerod. 155, 174–181.

Coudurier, C., Lepreux, O., Petit, N., 2018. Modelling of a tuned liquid multi-column damper. Application to floating wind turbine for improved robustness against wave incidence. Ocean Eng. 165, 277–292.

Hirt, C.W., Nichols, B.D., 1981. Volume of fluid (VOF) method for the dynamics of free boundaries. J. Comput. Phys. 39 (1), 201–225.

Holden, C., Fossen, T.I., 2012. A nonlinear 7-DOF model for U-tanks of arbitrary shape. Ocean Eng. 45, 22–37.

Kerkvliet, M., Vaz, G., Carette, N., Gunsing, M., 2014. Analysis of U-type anti-roll tank using URANS: sensitivity and validation. In: ASME 2014 33rd International Conference on Ocean, Offshore and Arctic Engineering.

Lopez-Pavon, C., Souto-Iglesias, A., 2015. Hydrodynamic coefficients and pressure loads on heave plates for semi-submersible floating offshore wind turbines: a comparative analysis using large scale models. Renew. Energy 81, 864–881.

Murtagh, P., Ghosh, A., Basu, B., Broderick, B., 2008. Passive control of wind turbine vibrations including blade/tower interaction and rotationally sampled turbulence. Wind Energy: An International Journal for Progress and Applications in Wind Power Conversion Technology 11 (4), 305–317.

OpenFOAM, 2019. The OpenFOAM Foundation Website.

Ramírez, L., Fraile, D., Brindley, G., 2020. Offshore Wind in Europe: Key Trends and Statistics 2020.

Robertson, A., Jonkman, J., Masciola, M., Song, H., Goupee, A., Coulling, A., Luan, C., 2014. Definition of the Semisubmersible Floating System for Phase II of OC4. National Renewable Energy Lab.(NREL), Golden, CO (United States).

Ruiz, R.O., Lopez-Garcia, D., Taflanidis, A.A., 2016. Modeling and experimental validation of a new type of tuned liquid damper. Acta Mech. 227 (11), 3275–3294.

Sakai, F., 1989. Tuned liquid column damper-new type device for suppression of building vibration. In: Proc. Proceedings of 1st International Conference on High-Rise Buildings, pp. 926–931.

Sun, L., Fujino, Y., Pacheco, B., Chaiseri, P., 1992. Modelling of tuned liquid damper (TLD). J. Wind Eng. Ind. Aerod. 43 (1–3), 1883–1894.

Thanyamanta, W., Molyneux, D., 2012. Prediction of stabilizing moments and effects of U-tube anti-roll tank geometry using CFD. In: ASME 2012 31st International Conference on Ocean, Offshore and Arctic Engineering, pp. 503–512.

Trust, C., 2015. Floating Offshore Wind: Market and Technology Review," Prepared for the Scottish Government.

WindEurope, 2019. Our Energy, Our Future.

Xue, M.-A., Dou, P., Zheng, J., Lin, P., Yuan, X., 2022. Pitch motion reduction of semisubmersible floating offshore wind turbine substructure using a tuned liquid multicolumn damper. Mar. Struct. 84, 103237.

Yu, W., Cheng, P.W., 2020. Verification of a passive tuned liquid multi-column damper for floating wind turbine. In: Proc. The 30th International Ocean and Polar Engineering Conference. OnePetro.

Yu, J.K., Wakahara, T., Reed, D.A., 1999. A non-linear numerical model of the tuned liquid damper. Earthq. Eng. Struct. Dynam. 28 (6), 671–686.

Zhou, Y., Xiao, Q., Peyrard, C., Pan, G., 2021. Assessing focused wave applicability on a coupled aero-hydro-mooring FOWT system using CFD approach. Ocean Eng. 240, 109987.

Zhou, Y., Qian, L., Bai, W., Lin, Z., 2022a. Investigations on the effects of internal liquid sloshing of semi-submersible floating offshore wind turbines. In: International Conference on Offshore Mechanics and Arctic Engineering. American Society of Mechanical Engineers.

Zhou, Y., Xiao, Q., Liu, Y., Incecik, A., Peyrard, C., Wan, D., Pan, G., Li, S., 2022b. Exploring inflow wind condition on floating offshore wind turbine aerodynamic characterisation and platform motion prediction using blade resolved CFD simulation. Renew. Energy 182, 1060–1079.